Theoretical and experimental investigations on damper performance for suppression of thermoacoustic oscillations

Nicolas Noiray, Bruno Schuermans

Alstom Power, Baden, Switzerland

Abstract

This study deals with a generic approach for prediction of pulsation suppression with acoustic dampers. Although the theory is valid for any self-oscillating system and for any damper type, the focus in this paper is on suppression of thermoacoustic oscillations using Helmholtz dampers. The developed theory has been validated using a novel experimental method. In thermoacoustics the constructive interference between the heat release and the acoustic field is responsible for growth of acoustic amplitudes. In the newly developed measurement method, this interaction has been mimicked by a feedback excitation using loudspeakers and microphones. Non-linear time-domain acoustic network simulations are also used to support the analytical and experimental framework.

1. Introduction

Combustion instabilities are difficult to predict during the development phase of a new burner. If a combustor yields resonant coupling during conception phase, solutions may be found to efficiently suppress the pulsations. Addition of dampers is an efficient way to prevent from these self-induced oscillations [1, 2, 3].

Successful implementation of such passive solution is usually obtained from the adjustment of the damper eigenfrequency to the unstable mode, where acoustic absorption is maximized, and from expensive trial-and-error based tests to optimize the number and locations of dampers [4, 5].

Enhancement of modal damping by implementing arrays of dampers has been widely investigated (e.g. [6]). In a recent study [7], design criteria are proposed in order to maximize the acoustic absorption of an array of liquid propellant injectors in rocket engines, which can behave as half-wave resonators in addition to their original function of injection. In another interesting investigation [8], a general theoretical model allowing to predict the acoustic interaction between an enclosure and a Helmholtz resonator array is derived and validated with experimental data. In reference [9], the absorption properties of set of helmholz dampers is experimentally analyzed and it is shown that it exists an optimum number of resonators to maximize the damping of a given enclosure's eigenmode. These studies are concerned with the noise control of naturally "stable" reverberant enclosures and do not consider the situation of acoustically "unstable" system. Thermoacoustic

This is a pre-print version. Published in *Journal of Sound and Vibration* (2012) Vol. 331 (12), p. 2753-2763, DOI: 10.1016/j.jsv.2012.02.005

instabilities occuring in combustion chamber is a particular case of such unstable systems, where the resonant coupling between an acoustic source and the enclosure eigenmodes yield an exponential growth of acoustic perturbations.
In this context, the present work aims at (1) providing a general theoretical model allowing to predict the influence of a given set of Helmholtz resonators on a thermoacoustic instability, (2) validating the model experimentally in a simple configuration and (3) proposing an original, non-reacting and easy to handle setup to evaluate the ability of dampers to stabilize the system prior to their implementation. It must be emphasized that while the model validation is done in a cold flow experiment, the theory does equally apply to non-reactive and reactive situations. An acoustically unstable system is set up. It can be adjusted to any frequency and growth rate. This is achieved by making use of a feedback loop where a speaker, which acts as the acoustic source in an enclosure and is fed by an amplified-delayed microphone signal. The imposed delay and the amplification factor in the loop allow control of the growth rate, while the frequency of interest is selected by means of an analog filter in this loop. In this way it is possible to mimic the characteristics of a given thermoacoustic instability in a simple cold flow setup and test the dampers capabilities.
The paper is organized as follows:

- The theoretical model is derived in the second section. Considering a system with given thermoacoustics characteristics, i.e. frequency and growth rate, the analytical model provides the stability properties of the same system equipped with dampers.
- In the third section, the experimental setup is detailed and the measurements are compared with the theoretical model.
- In the last section, a nonlinear time-domain acoustic network of the experimental setup is used in order to explain the differences between the analytical predictions and experimental results.

2. Theoretical model

The sketch given in Fig. 1 presents the connections between fluctuating quantities when thermoacoustic instabilities occur in a combustor. The variables ρ, Q', p' and $\boldsymbol{u'}$ respectively designate the gas density in the combustor volume V, the fluctuating component of the heat release, the acoustic pressure and the acoustic velocity; $s = i\omega + \nu$ is the Laplace variable, where ω is the angular frequency. The volumetric fluctuating heat release may be decomposed as $Q = Q'_N + Q'_C$ where Q'_C is the coherent component which is correlated to the acoustic velocity and/or pressure through the flame transfer function, and Q'_N the component independent of the acoustics (noise). The boundary conditions on the surface $S - S_d$ are expressed with the impedance Z. Dampers featuring an impedance Z_d can eventually be applied on the surface S_d.
Standing waves are considered here, and the acoustic variables p' and u' can be expressed as a

This is a pre-print version. Published in *Journal of Sound and Vibration* (2012) Vol. 331 (12), p. 2753-2763, DOI: 10.1016/j.jsv.2012.02.005

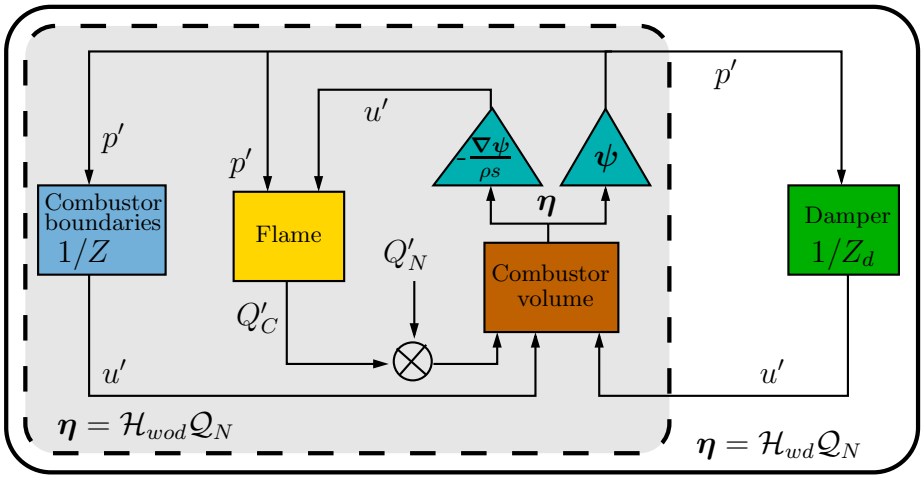

Figure 1: Schematic of a thermoacoustic system equipped with a damper.

superposition of expansion functions which constitutes a complete orthonormal basis $\boldsymbol{\psi}$ in the domain (see [10], p. 554-563). In the frequency domain, it is written as

$$\widehat{p}(s,\boldsymbol{x}) = \sum_{k=0}^{\infty} \eta_k(s)\psi_k(\boldsymbol{x}) \quad \text{and} \quad \widehat{\boldsymbol{u}}(s,\boldsymbol{x}) = -\frac{1}{s\bar{\rho}}\boldsymbol{\nabla}\widehat{p} = -\frac{1}{s\bar{\rho}}\sum_{k=0}^{\infty} \eta_k(s)\boldsymbol{\nabla}\psi_k(\boldsymbol{x}). \tag{1}$$

One can note that the schematic presented in Fig. 1 is a simplified interpretation which does not include for instance the vortex sound sources or which does not highlight elementary mechanisms involved in the flame transfer function (vortex flame interaction, equivalence ratio perturbations triggered by acoustic excitation, etc), but these can of course easily be included in such a general framework.

We focus now on the transfer functions linking the expansion amplitude vector $\boldsymbol{\eta} = [\eta_1 \dots \eta_n \dots \eta_\infty]$ to a function $\mathcal{Q}_N$ of the non-coherent component of fluctuating heat release rate $\widehat{Q}_N$, with and without dampers : $\boldsymbol{\eta} = \mathcal{H}_{wd}\mathcal{Q}_N$ and $\boldsymbol{\eta} = \mathcal{H}_{wod}\mathcal{Q}_N$.

Choosing a suitable expansion basis and making use of adequate assumptions, it is possible to derive simple expressions for $\mathcal{H}_{wod}$ and $\mathcal{H}_{wd}$ and this is the purpose of the present section.

The acoustic propagation in the volume V bounded by the surface S is described with 1) the homogeneous Helmholtz equation in a uniform low Mach flow with a fluctuating heat release source and 2) the boundary condition on S :

$$\nabla^2\widehat{p}(s,\boldsymbol{x}) - \left(\frac{s}{\bar{c}}\right)^2 \widehat{p}(s,\boldsymbol{x}) = -s\frac{\gamma-1}{\bar{c}^2}\widehat{Q}(s,\boldsymbol{x}) \quad \text{in } V, \tag{2a}$$

$$\text{and} \quad \frac{\widehat{p}(s,\boldsymbol{x})}{\widehat{\boldsymbol{u}}(s,\boldsymbol{x})\cdot\boldsymbol{n}} = Z(s,\boldsymbol{x}) \quad \text{on } S, \tag{2b}$$

This is a pre-print version. Published in *Journal of Sound and Vibration* (2012) Vol. 331 (12), p. 2753-2763, DOI: 10.1016/j.jsv.2012.02.005

where γ is the specific heat ratio, $\bar{c}$ the mean sound speed, $\boldsymbol{n}$ the outward normal on S and Z the acoustic impedance. Making use of a Green function, which is defined in the frequency domain by

$$\nabla^2 \widehat{G}(\boldsymbol{x}|\boldsymbol{x}_0) - \left(\frac{s}{\bar{c}}\right)^2 \widehat{G}(\boldsymbol{x}|\boldsymbol{x}_0) = \delta(\boldsymbol{x}-\boldsymbol{x}_0) \quad \text{in } V, \tag{3a}$$

$$\text{and} \quad \boldsymbol{\nabla}\widehat{G}(\boldsymbol{x}|\boldsymbol{x}_0)\cdot\boldsymbol{n} = g(\boldsymbol{x}) \quad \text{on } S, \tag{3b}$$

it is possible to write an expression for the fluctuating pressure at a point $\boldsymbol{x}$ in the domain. To do so, one has to substract (3a) multiplied by $\widehat{p}$ to (2a) multiplied by $\widehat{G}$, integrate the resulting equation over the volume, make use of the boundary conditions (2b) and (3b), and of the symmetry property of the Green function $\widehat{G}(\boldsymbol{x}_0|\boldsymbol{x}) = \widehat{G}(\boldsymbol{x}|\boldsymbol{x}_0)$[1], which yields

$$\begin{aligned}\widehat{p}(s,\boldsymbol{x}) = -s\frac{\gamma-1}{\bar{c}^2}\int_V \widehat{G}(\boldsymbol{x}_0|\boldsymbol{x})\widehat{Q}(s,\boldsymbol{x}_0)dV_0 + \int_S \widehat{p}(s,\boldsymbol{x}_0)g(\boldsymbol{x_0})dS_0 \\ + \int_S \widehat{G}(\boldsymbol{x}_0|\boldsymbol{x})s\bar{\rho}\frac{\widehat{p}(s,\boldsymbol{x}_0)}{Z(s,\boldsymbol{x}_0)}dS_0.\end{aligned} \tag{4}$$

The Green function is now spanned on an orthonormal basis $\boldsymbol{\psi}$: $\widehat{G}(\boldsymbol{x}|\boldsymbol{x}_0) = \sum_{j=0}^{\infty} A_j\psi_j(\boldsymbol{x})$. The basis functions ψ_j are defined as

$$\nabla^2\psi_j + \left(\frac{\omega_j}{\bar{c}}\right)^2\psi_j = 0 \quad \text{in } V, \tag{5a}$$

$$\begin{aligned}&\boldsymbol{\nabla}\psi_j\cdot\boldsymbol{n} = g \quad \text{on } S, \\ &\text{with } \int_V \psi_n\psi_m^* dV = V\Lambda_n\delta_{nm}, \text{ and } \Lambda_n = \frac{1}{V}\int_V |\psi_n|^2 dV\end{aligned} \tag{5b}$$

Replacing $\widehat{G}$ in (3a) by its expanded form, multiplying by ψ_m^*, integrating over the volume V and making use of the basis function definition (5a) and of the orthogonality of the basis, one obtains the coefficient A_m, and one can write :

$$\widehat{G}(\boldsymbol{x}|\boldsymbol{x}_0) = \sum_{j=0}^{\infty}\psi_j(\boldsymbol{x})\frac{\psi_j^*(\boldsymbol{x}_0)\bar{c}^2}{-V\Lambda_j(\omega_j^2+s^2)} \tag{6}$$

Replacing $\widehat{G}$ in (4) by the r.h.s. of (6) yield

$$\widehat{p}(s,\boldsymbol{x}) = \sum_{j=0}^{\infty}\eta_j(s)\psi_j(\boldsymbol{x}) \tag{7}$$

[1] i.e. the wave observed at $\boldsymbol{x}$ due to a point source at $\boldsymbol{x}_0$ has the same amplitude and relative phase as for the wave observed at $\boldsymbol{x}_0$ when the point source is located at $\boldsymbol{x}$

This is a pre-print version. Published in *Journal of Sound and Vibration* (2012) Vol. 331 (12), p. 2753-2763, DOI: 10.1016/j.jsv.2012.02.005

where the expansion amplitude vector coefficients are defined as solutions of

$$\eta_j = \frac{s\bar{\rho}\,\bar{c}^2}{s^2+\omega_j^2}\,\frac{1}{V\Lambda_j}\Bigg(\overbrace{\frac{\gamma-1}{\bar{\rho}\,\bar{c}^2}\int_V \widehat{Q}_N\psi_j^* dV}^{\text{(A)}} + \overbrace{\frac{\gamma-1}{\bar{\rho}\,\bar{c}^2}\int_V \widehat{Q}_C(\boldsymbol{\eta},\boldsymbol{\psi})\psi_j^* dV}^{\text{(B)}} - \underbrace{\frac{1}{s\bar{\rho}}\int_S g\sum_{k=0}^{\infty}\eta_k\psi_k dS}_{\text{(C)}} - \underbrace{\int_{S-S_d}\frac{\sum_{k=0}^{\infty}\eta_k\psi_k}{Z}\psi_j^* dS}_{\text{(D)}} - \underbrace{\int_{S_d}\frac{\sum_{k=0}^{\infty}\eta_k\psi_k}{Z_d}\psi_j^* dS}_{\text{(E)}}\Bigg) \tag{8}$$

The infinite set of equations defining the amplitude vector $\boldsymbol{\eta}$ is general. Whatever the chosen basis $\boldsymbol{\psi}$, it is theoretically possible to retrieve the amplitude coefficients (e.g. [13], Appendix F), and it is thus possible to numerically get approximate solution by considering a finite set of basis functions. The idea is now to derive a simple analytical formulation of η_j, where the interdependency of the coefficients is removed, by making use of the following assumptions :

- The functions $\psi_j(\boldsymbol{x})$ composing the orthonormal basis $\boldsymbol{\psi}$ are suitably defined to be similar to the acoustic eigenmodes spatial distribution of the system without acoustic sources.
- From the acoustic viewpoint, the system comprises either quasi-closed or quasi-open boundaries, and the definition of $\boldsymbol{\psi}$ yield the integral (C) to vanish[2].
- One consider that the thermoacoustic coupling operates on a single eigenmode – the one featuring the largest linear growth rate for linearly unstable systems (see for example [14]) – and that one can write $\eta_m \simeq 0$ for $m \neq j$.
- The volume source/sink integral (B) – due to the constructive/destructive interaction between the coherent fluctuating heat release rate and the acoustics – and the boundary integral (D) – defined by the actual impedance at the boundaries ($S - S_d$) – are small, does not dramatically change the eigenmodes spatial distribution and eigenfrequencies, and can

[2]For instance, one can consider the simple one-dimensional case of a duct of length L with an acoustic source.
If the duct is closed at both ends – which is not far from the boundary conditions encountered in gas turbine combustor (high acoustic reflection coefficients of the inlet and of the outlet) – it is appropriate to define the basis function such as $\boldsymbol{\nabla}\psi_j \cdot \boldsymbol{n} = g = 0$ at the boundaries, which is satisfied with $\psi_j(x) = \cos(xj\pi/L)$. This means that the fluctuating velocity should tend to zero at the boundaries (see eq. (1)), and $g = 0$ yields vanishing (C) in eq. (8).
If the duct is open at both ends – typical configuration of the Rijke tube – it is now appropriate to define the basis function such as $\psi_j = 0$ at the boundaries, which is satisfied with $\psi_j(x) = \sin(xj\pi/L)$. This means that the fluctuating pressure should tend to zero at the boundaries (see eq. (1)), and this also yields vanishing (C) in eq. (8).
If now the duct is open at one end and closed at the other, it is now appropriate to use the basis function $\psi_j(x) = \sin(x(2j-1)\pi/2L)$ which satisfied $\psi_j = 0$ at the first boundary and $g = 0$ at the second and thus (C)=0.

This is a pre-print version. Published in *Journal of Sound and Vibration* (2012) Vol. 331 (12), p. 2753-2763, DOI: 10.1016/j.jsv.2012.02.005

be replaced by adding growth/decrease rate coefficient $-2\nu_j s$ in the denominator of the first r.h.s. fraction (with $\omega_j \gg \nu_j$). This growth rate can be estimated in practical configurations by using modal identifications techniques from the acoustic pressure measurements.

It can be pointed out that the eigenmodes of a thermoacoustic system are by nature non-normal [11]. Also, in the general case, it was shown in [12] that systems with complex impedances at the boundaries admit non-normal eigenmodes. In the present analysis the system eigenmodes are expanded on an orthonormal basis. Using this Galerkin technique with orthonormal basis functions ψ_j does not mean that the eigenmodes will also be orthogonal so eq. 8 is always valid. However, keeping only one basis function for the instability description and stating that it does not significantly differs from the unstable eigenmode is an assumption which goes against the theoretical work presented in refs. [11] and [12]. This assumption is done for two reasons: (1) In many practical systems, the thermoacoustic coupling is usually weak ($\omega_j \gg \nu_j$), the surface S_d where dampers with complex impedance are applied is small compared to the overall boundary and the observed eigenmodes are not much different than the one calculated from non-active flames. (2) Considering the modal non-normality is mostly useful for linearly stable systems which could exhibit a non-linear instability due to triggering of periodic stable state by transient linear growth. In the present analysis we only consider systems which are already unstable and do not admit nonoscillating equilibria.
The eigenmode amplitude η_j is then given by

$$\eta_j(s) \simeq \frac{s\bar{\rho}\,\bar{c}^2}{s^2 - 2\nu_j s + \omega_j^2}\,\frac{1}{V\Lambda_j}\left(\frac{\gamma-1}{\bar{\rho}\,\bar{c}^2}\int_V \widehat{Q}_N(s,\boldsymbol{x})\psi_j^*(\boldsymbol{x})dV - \int_{S_d}\eta_j(s)\frac{|\psi_j(\boldsymbol{x})|^2}{Z_d(s,\boldsymbol{x})}dS\right) \tag{9}$$

Considering now the particular case of nearly closed system (Green function expansion basis defined with $g = 0$, yielding $(\psi_j, \omega_j) \in \mathbb{R}^2$), where $S_d = 0$, one can write

$$\begin{gathered}\eta_j(s) = \mathcal{H}_{wod}\mathcal{Q}_N,\\ \text{where}\quad \mathcal{H}_{wod} = \frac{s\,\omega_j/q_j}{s^2 + s\,\omega_j/q_j + \omega_j^2}\quad \text{with } q_j = -\omega_j/2\nu_j,\\ \text{and}\quad \mathcal{Q}_N = \tfrac{1}{-2\nu_j}\,\tfrac{\gamma-1}{V\Lambda_j}\int_V \widehat{Q}_N\psi_j dV\end{gathered} \tag{10}$$

Since $\omega_j \gg \nu_j$, the denominator of $\mathcal{H}_{wod}$ can be approximated by $(s - i\omega_j + \nu_j)(s + i\omega_j + \nu_j)$. When $\nu_j > 0$, and thus $q_j < 0$, the modal amplitude $\eta_j(t)$ (without dampers) is exponentially amplified at the rate ν_j, i.e. the system is linearly unstable, because the real part of the poles of the characteristic polynomial is positive. Similarly, when $q_j > 0$, the system without dampers is stable and the perturbations are damped.
A number N of identical damper of Helmholtz type are applied on S_d with $NA_d = S_d$, where A_d designates the surface of the mouth of a damper. These dampers are located at the coordinates $\boldsymbol{x}_k$

This is a pre-print version. Published in *Journal of Sound and Vibration* (2012) Vol. 331 (12), p. 2753-2763, DOI: 10.1016/j.jsv.2012.02.005

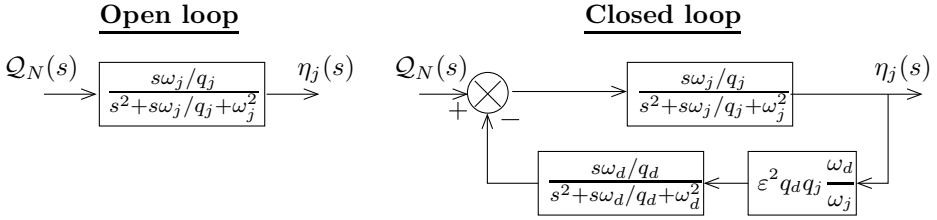

Figure 2: Block diagrams of the stand alone system and of the damper equipped system.

and are supposed to 1) feature a constant impedance over A_d and 2) be compact with respect to the wavelength associated to the mode considered ($\sqrt{A_d} \ll \lambda_j$), which means that the eigenfunction $\psi_j(\boldsymbol{x}_k)$ is also constant over A_d. Combining then (9) and (10), one obtains :

$$\eta_j(s) = \mathcal{H}_{wod}\mathcal{Q}_N - \mathcal{H}_{wod}\frac{\bar{\rho}\,\bar{c}^2}{\omega_j/q_j}\,\frac{A_d\,\sum_{k=1}^{N}\psi_j^2(\boldsymbol{x}_k)}{Z_d\,V\Lambda_j}\,\eta_j(s) \tag{11}$$

The dampers are designed to suppress the eigenmode corresponding to ψ_j and are working on the Helmholtz mode (damped harmonic oscillator) over the frequency range considered. Their impedance can be written with a classical 2^{nd} order transfer function

$$\frac{1}{Z_d(s)} = \frac{s\,\omega_d/q_d}{s^2 + s\,\omega_d/q_d + \omega_d^2}\,\frac{q_d\,V_d\,\omega_d}{\bar{\rho}_d\,\bar{c}_d^2\,A_d} \tag{12}$$

In these expressions, $\bar{\rho}_d$ and $\bar{c}_d$ designate the mean density and sound speed in the dampers, V_d and A_d the damper volume and mouth area, and ω_d and q_d the Helmholtz angular frequency and the damping factor.

We now introduce $\varepsilon = (\bar{\rho}_d\,V_d\,\sum_{k=1}^{N}\psi_j^2(\boldsymbol{x}_k)/\bar{\rho}\,V\Lambda_j)^{1/2}$. The nondimensional parameter ε may be described as a damping efficiency factor depending on the dampers to combustor volume ratio and on their location with respect to the eigenmode shape similar to ψ_j. Noting that $\bar{\rho}_d\;\bar{c}_d^2 \simeq \bar{\rho}\;\bar{c}^2$, and combining (11) and (12), one finally obtains the link between η_j and $\mathcal{Q}_N$, which stands for the closed-loop transfer function $\mathcal{H}_{wd}$ describing the combustor equipped with the dampers. This closed-loop is presented in Fig. 2, where the dampers act as feedback control.

For a given unstable system featuring a mode shape ψ_j, an eigenfrequency ω_j and a growth rate ν_j, it is possible to extract the eigenfrequency ω and growth rate ν corresponding to the system equipped with dampers, as function of their locations and characteristics i.e. as function of ω_d, q_d and ε. The solution $s = i\omega + \nu$ is the eigenvalue of the closed loop system in Fig. 2.

Considering a well instrumented pulsating combustor, the frequency ω_j, the growth rate ν_j and the mode shape ψ_j can be deduced by means of dynamic pressure sensors. It is then possible to develop dampers featuring an impedance Z_d, and use the model to predict how many of these dampers are required and where they have to be implemented in order to stabilize the system at the frequency ω_j. In other words, if the eigenvalue of the closed loop features a negative real

This is a pre-print version. Published in *Journal of Sound and Vibration* (2012) Vol. 331 (12), p. 2753-2763, DOI: 10.1016/j.jsv.2012.02.005

part $\nu < 0$, the system which was initially unstable $\nu_j > 0$ is predicted to be stable with the dampers. The objective is now to demonstrate that growth rate reduction, due to the damper implementation, predicted by the model is in agreement with what is observed experimentally.

3. Experimental setup

While the theoretical model has a general feature and can be applied to any combustor and eigenmode shape, the validation is here carried out in a basic configuration where a rectangular cavity, with its longitudinal eigenmodes, is considered. This configuration allows to validate the model in a simpler way. In order to mimic thermoacoustic instabilities, an electro-acoustic feedback is implemented in a closed tube to generate self-induced oscillations at the desired frequency and growth rate.

The setup is sketched in Fig. 3. The left side of tube is equipped with a low porosity perforated plate featuring a high reflection coefficient ($R_1 \simeq 0.95$ over the frequency range considered, with and without flow) followed by an anechoic end (made of acoustic foam) and an exhaust pipe. On the right side is mounted either a wall ($R_2 = 1$) or a damper with an air inlet. The length of the resulting cavity, in which the acoustic modes are considered, is L, and the square duct side is equal to l.

A wall equipped with a set of N_d tiny Helmholtz resonators constitutes the damper. Their volume and mouth area are V_d and A_d. The reflection coefficient of the damper $R_d = (Z_d - \rho c)/(Z_d + \rho c) = g/f$, where f and g are the upward and downward Riemann invariants ($p'/\rho c = f + g$ and $u' = f - g$), was measured by means of the multi-microphone technique and is presented in Fig. 4. The parameters ω_d and q_d of the second order model of the resonator impedance, given in eq. (12), are optimized such that the reflection coefficient model best fits the measured data (see green line in Fig. 4 where $q_d = 2.2$). It appears that these optimum parameters are of the order of those that can be obtained from the existing literature (e.g. [15] p. 137-140) and are therefore used for the calculations performed in the last section. In order to generate the self-induced acoustic oscillations in the cavity of length L, a feedback loop is used as shown in Fig. 3. A switch button is used to run the feedback loop. When it is switched on, the pressure signal recorded with the microphone is filtered (Analog filter, Krohn-Hite 3343), amplified (1^{st} channel of the Compressor, Alesis 3630), delayed (Delay generator, Yamaha D5000), limited when the amplitude exceeds a defined threshold (2^{nd} channel of the Compressor, Alesis 3630) and used to feed the compression driver which is plugged on the other side of the impedance tube. When the loop is switched on, several eigenmodes are unstable. We consider here the longitudinal modes : eigenfrequency $f_j = \omega_j/2\pi = nc/2L$ (with $n = 1, 2, ...$), where $f_j < c/2l$. These linearly unstable modes feature growth rates which depend on the amplification factor and on the delay imposed. Without any filter in the feedback loop, the most unstable one, i.e. the one featuring the largest linear growth rate, would start to growth. The filter is indeed used to select unstable modes that are in the frequency range of interest. The amplitude limiter is included in the loop in order 1) to reproduce

This is a pre-print version. Published in *Journal of Sound and Vibration* (2012) Vol. 331 (12), p. 2753-2763, DOI: 10.1016/j.jsv.2012.02.005

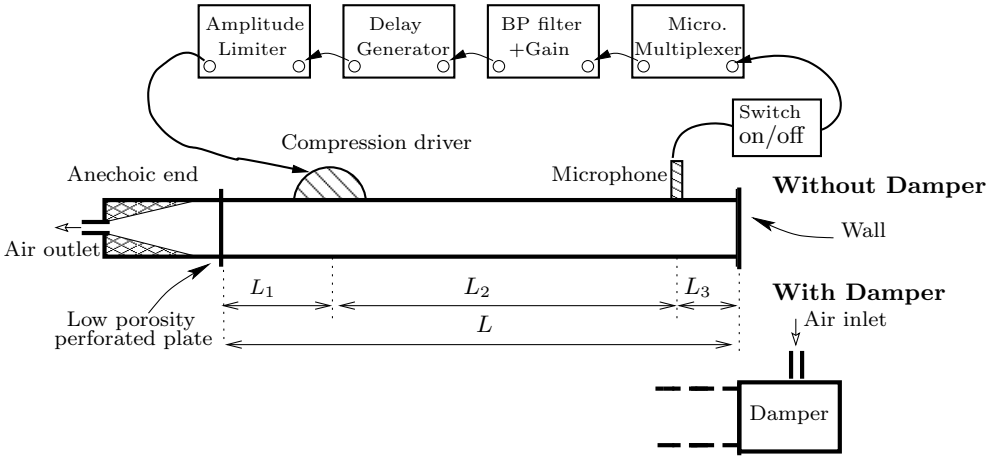

Figure 3: Sketch of the experimental setup used to produce self-induced acoustic oscillations.

nonlinear flame response saturation for high acoustic levels, and 2) from a practical viewpoint, to avoid breaking the compression driver with an overload due to the exponential growth of the feeding signal for unstable cases. Two unstable modes ($\omega_j/\omega_d \simeq 0.85$ and $\omega_j/\omega_d \simeq 1.14$) will be considered for the validation of the theoretical model given in Fig. 2. The electro-acoustic instabilities are first run without dampers, at an eigenfrequency f_j selected with the analog filter, and for different growth rates ν_j which are adjusted by changing the feedback loop delay τ_F. In a second step, setting the same hardware parameters – i.e. the ones used to produce self-induce oscillation at ω_j and ν_j – the loop is run in presence of damper in order to obtain the growth rate reduction due to the damper acoustic energy absorption.

For this experimental validation, it is more convenient to measure growth rates ($\nu > 0$) than decrease rate ($\nu < 0$), so a high gain in the feedback-loop is required to get self-induced oscillations for both situations. In other words, at the eigenfrequencies of interest, the damper is not effective enough to stabilize the system and it is possible to quantitatively measure the growth rate reduction from the case without to the case with damper.

An example of measurement with and without damper for the eigenfrequency $\omega_j/\omega_d \simeq 1.14$ is given in Fig. 5. Growth rate measurements are done by taking the mean increase over the linear growth phase. In Fig. 5, The growth rate reduction is clearly exemplified: $\nu_{\mathrm{wod}}/\omega_d \simeq 9 \times 10^{-3}$ without damper and $\nu_{\mathrm{wd}}/\omega_d \simeq 3.6 \times 10^{-3}$ with damper where the phase delay is set to $\omega_d \tau_F = 3.6$. Note, there is obviously a modulation of the amplitude superimposed to the exponential growth and to the limit cycle. This phenomenon will be discussed and explained in the following section. In particular, it will be shown that the mean linear growth rates (red bold lines in Fig. 5) can be used for the growth rate reduction analysis.

Growth rates have been measured in the same way for a set of feedback-loop delays and the results

This is a pre-print version. Published in *Journal of Sound and Vibration* (2012) Vol. 331 (12), p. 2753-2763, DOI: 10.1016/j.jsv.2012.02.005

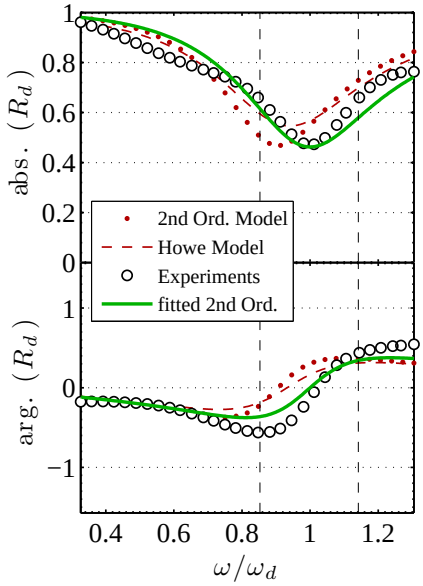

Figure 4: Reflection coefficient of the damper which was used in the present study.

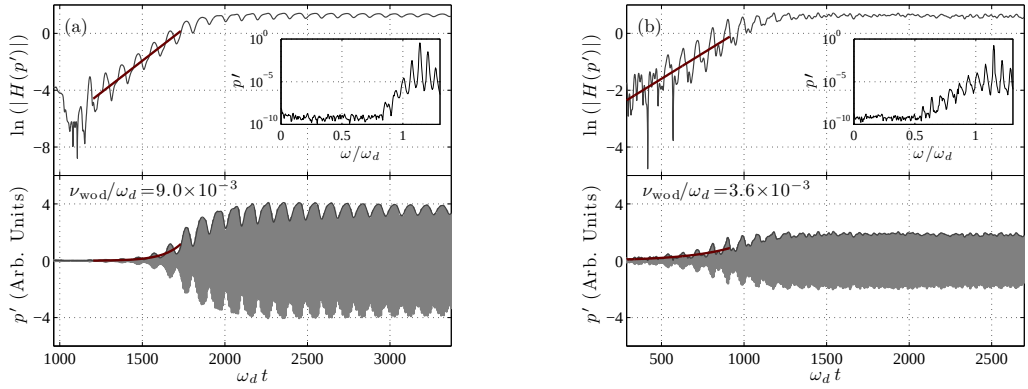

Figure 5: **(a)** Experiment without damper (with $\omega_d\tau_F = 3.6$). **(b)** Experiment with damper (with $\omega_d\tau_F = 3.6$). Examples of measured signals. Lower subfigures : (1) grey thin line : pressure signal, (2) black thin line : amplitude deduced from the pressure Hilbert transform $|H(Re(p'))|$, (3) red bold line : fitted exponential growth. Upper subfigures : (2) black thin line : logarithm of the amplitude, (2) red bold line : fitted logarithm of the exponential growth $\Rightarrow$ linear evolution and (3) amplitude spectrum of the pressure.

are reported and compared to the theoretical model in Fig. 6. The growth rates with damper $\nu_{\rm wd}$ are plotted as function of the ones without damper $\nu_{\rm wod}$ for several delays and for two eigenmodes ($\omega_j/\omega_d \simeq 0.85$ and $\omega_j/\omega_d \simeq 1.14$). For each delay, four measurements were done, providing a

This is a pre-print version. Published in *Journal of Sound and Vibration* (2012) Vol. 331 (12), p. 2753-2763, DOI: 10.1016/j.jsv.2012.02.005

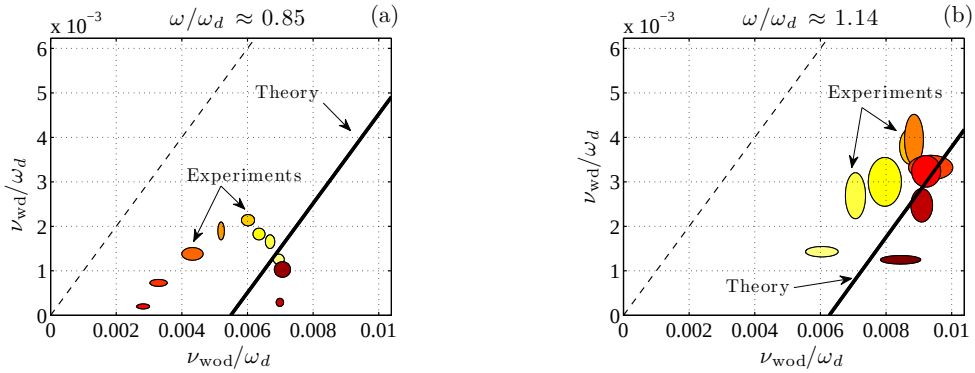

Figure 6: Experimental results : **(a)** the eigenfrequency corresponds to $\omega_j/\omega_d \simeq 0.85$ and **(b)** to $\omega_j/\omega_d \simeq 1.14$. Each colored region in the upper diagrams corresponds to a given delay, is centered at the mean coordinate $[\nu_{\rm wod}; \nu_{\rm wd}]$ obtained from 4 successive measurements, with an extent defined by the standard deviation.

mean growth rate with a standard deviation. Both frequencies and growth rates are dependent on the imposed delays. The theoretical predictions (bold dark lines) are obtained from the model (see Fig. 2) by calculating the closed-loop system eigenvalues while fixing : ω_d; $\omega_j/\omega_d = 0.85$; $q_j \in]-\infty; -42.5] \Leftrightarrow \nu_j/\omega_d \in [0; 0.01]$ (resp. $q_j \in]-\infty; -57]$ for $\omega_j/\omega_d = 1.14$); $q_d = 2.2$; $\varepsilon = 8.7 \times 10^{-2}$ where $\Lambda_j = 1/V \int_V \psi_j^2 dV = 1/L \int_0^L \cos^2(n\pi x/L)dx = 1/2$.
In contrast with the measurements, for which the trajectories defined by the points $[\nu_{\rm wod}(\tau_F), \nu_{\rm wd}(\tau_F)]$ feature elliptical shapes, the model predictions exhibit linear relationships between $\nu_{\rm wd}$ and $\nu_{\rm wod}$. The major axis of the ellipses coincide with the bold dark lines calculated from the theoretical model. These results indicates that the model is apparently able to provide good estimates the mean growth rate reduction.
In the next section, acoustic network simulations of the experimental setup are presented. Simulating the delayed electro-acoustic feedback used in the experiments will allow to:

1. Explain the amplitude modulation during the exponential growth shown in Fig. 5 and justify the use of the measured mean linear growth rate for the comparison with the theoretical model.
2. Get a better understanding of the elliptical trajectories obtained when the measured growth rates are plotted against each other, and give additional informations on the model capabilities and limitations.

4. Acoustic network simulations of the experimental configuration

A simplified acoustic network representation of the experimental setup is now considered (see Fig. 7). The network is built using the Simulink® environment. Note, it is not intended here to accurately represent the experimental setup but more to get a better understanding of the

This is a pre-print version. Published in *Journal of Sound and Vibration* (2012) Vol. 331 (12), p. 2753-2763, DOI: 10.1016/j.jsv.2012.02.005

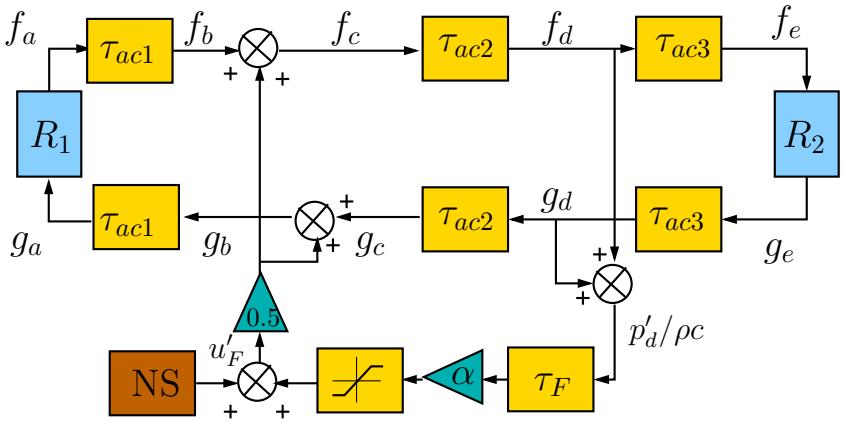

Figure 7: Acoustic network model of the experimental setup used to compute time domain simulations (Simulink representation). R_1 and R_2 are the upstream and downstream boundary conditions of the cavity (see Fig. 3), f and g the Rieman invariants at the different locations. Transport delay blocks are used to model the delays associated to the acoustic wave propagation in the cavity $\tau_{ac_i} = L_i/c$ and the delay imposed in the feedback loop τ_F. α is the amplification factor.

instability mechanism. For instance, the electro-acoustic conversion of the compression driver is simply modeled by an acoustic velocity source in the network. The normalised pressure $p'_d/\rho c = f_d + g_d$ measured with the microphone, is delayed by τ_F, amplified by a factor α (including the Pascal/Voltage conversion and the different gains in the loop, including the speakers transfer function), limited when it exceeds a defined threshold and sent back in the duct from the speaker as an acoustic velocity source[3] (conversion factor also included in α). The NS block in the feedback loop stands for the filtered noise source. The upstream reflection coefficicient can be either set to 1 for the wall boundary condition, or to $R_2 = R_d = (Z_d - \rho c)/(Z_d + \rho c)$ with Z_d defined in Eq. (12), for the damper boundary condition.

An example of time domain simulation of the network presented in Fig. 7 is given in Fig. 8. It was done with $R_1 = 0.95$, $R_2 = 1$, $\alpha = 0.2$ and $\omega_d \tau_F = 7.2$. The noise source was filtered with a narrow bandpass filter (-3dB attenuation cut-off frequencies : $\omega_1/\omega_d = 0.82$ and $\omega_2/\omega_d = 0.88$). Under these conditions, the system is unstable and one can see the exponential growth at a rate of $\nu_j/\omega_d = 2.7 \times 10^{-3}$ of the eigenmode at the frequency $\omega_j/\omega_d = 0.84$, followed by the saturation due to the amplitude limiter in the loop. The same simulation was done with a wider band-pass filter ($\omega_1/\omega_d = 0.78$ and $\omega_2/\omega_d = 0.92$). The resulting signal, given in Fig. 8, shows that

[3]One can write at the speaker location

$$f_c = f_b + u'_F/2 \quad \text{and} \quad g_b = g_c + u'_F/2,$$

Adding these two equations, one gets the mass flow conservation

$$f_c - g_c = f_b - g_b + u'_F \quad \Leftrightarrow \quad u'_c = u'_b + u'_F$$

where u'_F is the acoustic velocity source provided by the speaker.

This is a pre-print version. Published in *Journal of Sound and Vibration* (2012) Vol. 331 (12), p. 2753-2763, DOI: 10.1016/j.jsv.2012.02.005

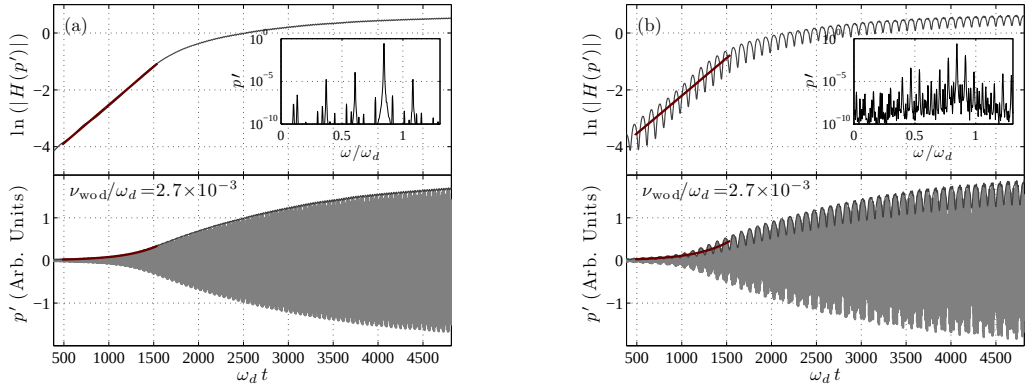

Figure 8: **(a)** Narrow band noise source ($\omega_1/\omega_d = 0.82$ and $\omega_2/\omega_d = 0.88$). **(b)** Wider band noise source ($\omega_1/\omega_d = 0.78$ and $\omega_2/\omega_d = 0.92$). Time domain simulation results. Lower subfigures : (1) grey thin line : pressure signal, (2) black thin line : amplitude deduced from the pressure Hilbert transform $|H(Re(p'))|$, (3) red bold line : fitted exponential growth. Upper subfigures : (2) black thin line : logarithm of the amplitude, (2) red bold line : fitted logarithm of the exponential growth $\Rightarrow$ linear evolution and (3) amplitude spectrum of the pressure.

1. The exponential growth and the limit cycle feature a low frequency amplitude modulation,
2. the mean growth rate remains the same as the one obtained with a narrow band filtered noise source.

The same kind of amplitude modulation was observed experimentally (see Fig. 5). It can therefore be assumed that the actual width of the analog band-pass filter used in the experiments is not narrow enough to prevent from this phenomenon. Moreover, it was relevant in the previous section to use the mean growth rates extracted from the modulated growths, since it is shown here that the ones extracted from pure exponential growths and obtained with an "ideal" filter would be the same.

Another way of extracting the growth rate $\nu_j/\omega_d = 2.7 \times 10^{-3}$, is to compute the eigenvalues of the network presented in Fig. 7 and get the imaginary part of the one corresponding to the eigenfrequency $\omega_j/\omega_d = 0.84$. This was done for several delays τ_F and for both condition $R_2 = 1$ and $R_2 = R_d$. The growth rates with damper ν_{wd} of the mode featuring an eigenfrequency close to $\omega_j/\omega_d = 0.84$, are plotted against the ones without damper ν_{wod} for several delays in Fig. 9 (delay increase : color darken). As explained in the figure's caption, the shaded regions define the stability regions, with linearly unstable (resp. stable) regions when the growth rate are positive (resp. negative). The theoretical predictions (bold dark line) are calculated for $\omega_j/\omega_d = 0.84$, $\nu_j/\omega_d \in [-0.015; 0.015]$, $q_d = 2.2$ and $\varepsilon = 8.7 \times 10^{-2}$.

These computations were done for two different amplification factor $\alpha = 0.1$ and $\alpha = 0.6$ (Fig. 9). The following conclusions can be sorted out from these numerical results :

1. For both cases, an excellent agreement is found between the theoretical predictions and the acoustic network model results.

This is a pre-print version. Published in *Journal of Sound and Vibration* (2012) Vol. 331 (12), p. 2753-2763, DOI: 10.1016/j.jsv.2012.02.005

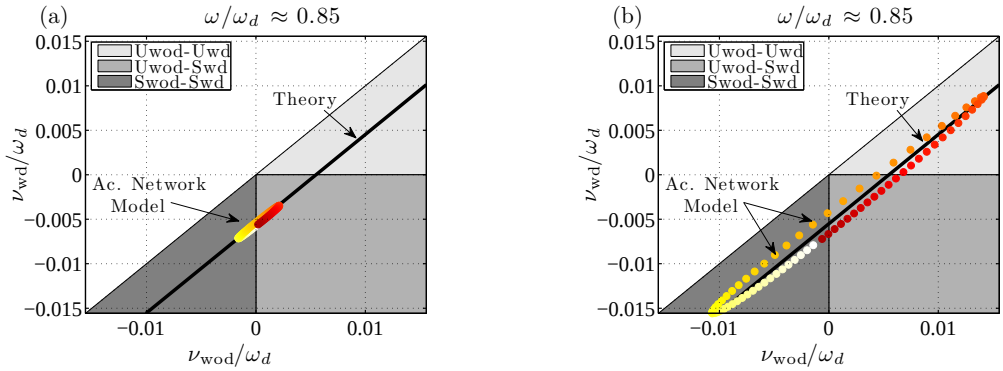

Figure 9: **(a)** Small amplification factor ($\alpha = 0.1$). **(b)** Large amplification factor ($\alpha = 0.6$). Damping efficiency prediction of the damper obtained from the theoretical model (bold black lines), and from the acoustic network description of the experimental setup as colored circles. Shaded regions: Uwod-Uwd for Unstable without damper and Unstable with damper, Uwod-Swd for Unstable without damper and Stable with damper, Swod-Swd for Stable without damper and Stable with damper.

2. For low feedback-loop amplification factor, since the damping is efficient ($\approx 5\times10^{-3}$ reduction due to the damper), the growth rates of the system with damper are always negative meaning that the system is linearly stable for all delays τ_F.
3. For large feedback amplication ($\alpha = 0.6$ in Fig. 9, right diagram), the system is still unstable with the dampers for a range of delays, and the elliptical shape of the trajectory can be clearly identified.

The elliptic-like deviation is all the more marked when the gain is large. This observation allows to explain the experimental results considering that the gain used for the measurements were high in order to get solutions in the "Unstable without damper and Unstable with damper" region.
It is now interesting to focus on these elliptic trajectories obtained when plotting the growth rates against each other, and try to explain this latter result by means of a linearized analytical model of this particular one dimensional electro-acoustic system. It can be shown that when $R_1 = R_2 = 1$ and $L_2 = L$ (i.e. $L_1 = L_3 = 0$), the first order approximation of the eigenfrequency of the system[4] is written as $\omega = \omega_0 + (-1)^n\alpha(-\sin(\omega_0\tau_F) + i\cos(\omega_0\tau_F))/\tau_L$, where $\omega_0 = 2\pi f_0 = nc\pi/L$. This result highlights the fact that both frequency $\mathrm{Re}(\omega)$ and growth rate $\mathrm{Im}(\omega)$ depend on the feedback-loop delay and on the amplification factor. The expression for the growth rate is then :

[4]With $L_1 = L_3 = 0$ and $R_1 = R_2 = 1$, one can write $f_d = f_e = g_e = g_d$ and $g_b = g_a = f_a = f_b$ and also $f_c = f_b + f_d\alpha\exp(i\omega\tau_F)$, $g_c = f_b - f_d\alpha\exp(i\omega\tau_F)$, $f_c = \exp(-i\omega\tau_L)f_d$ and $g_c = \exp(i\omega\tau_L)f_d$, which yields

$$\begin{pmatrix} 1 & \alpha e^{i\omega\tau_F} - e^{-i\omega\tau_L} \\ 1 & -\alpha e^{i\omega\tau_F} - e^{i\omega\tau_L} \end{pmatrix} \begin{pmatrix} f_b \\ f_d \end{pmatrix} = \begin{pmatrix} 0 \\ 0 \end{pmatrix}$$

The non-trivial solutions are obtained when the matrix determinant G satisfy $G(\omega,\alpha) = \alpha e^{i\omega\tau_F} + i\sin(\omega\tau_L) = 0$. Considering the eigenfrequency ω_0 such as $G(\omega_0, 0) = 0$, a gain $\alpha \ll 1$, and defining $\omega = \omega_0 + \omega_1$, where $\omega_1 \ll \omega_0$,

This is a pre-print version. Published in *Journal of Sound and Vibration* (2012) Vol. 331 (12), p. 2753-2763, DOI: 10.1016/j.jsv.2012.02.005

$\nu_{\text{wod}} = (-1)^n \alpha/\tau_L \cos(\omega_{0,\text{wod}}\tau_F)$, with the subscript "wod" standing for the case without damper. The same kind of dependence is observed when the case $R_2 = R_d \exp(i\varphi_d)$ is considered. It is therefore possible to perform the same derivation for any complex reflection coefficient R_2. The eigenfrequency is now $\omega_{0,\text{wd}} = \omega_{0,\text{wod}} - (\varphi_d + i\ln(1/R_d))/2\tau_L$. It is then possible to express the growth rate of the system with damper as function of the growth rate without damper [5]:

$$\begin{gathered} \nu_{\text{wd}} = C_1 + C_2 \left(C_3 \nu_{\text{wod}} + C_4 \sqrt{1 - (\tau_L/\alpha)^2 \nu_{\text{wod}}^2} \right) \\ \text{where} \quad C_1 = -\frac{\ln(1/R_d)}{2\tau_L}, \quad C_2 = (4R_d)^{-1/2}, \quad C_3 = (1+R_d)\cos(\varphi_d/2) \\ \text{and} \quad C_4 = (-1)^n \frac{\alpha}{\tau_L}(1-R_d)\sin(\varphi_d/2) \end{gathered} \tag{13}$$

This relationship between the growth rate with and without damper is a conic section, which explains the elliptical shape obtained. One can note that the evaluation of this first order derivation, not shown here, matches with the numerical simulation results shown in Fig. 9.
It has been shown that the stability nature of the electro-acoustic system which is considered in the previous sections can be modeled with simple equations. In the case of practical large-scale combustors, for which testing of dampers is costly, such basic description is generally not so accurate. The use of advanced thermo-acoustic tools including FEM analysis, lumped elements models and flame transfer functions deduced from CFD or experiments [16] is preferred and provide reliable predictions. The theoretical model proposed in the first section, which combines system identification and control approach, is an alternative strategy which requires less computing resources, can be applied to any complex thermo-acoustic system and provide good estimations of dampers performances.

5. Conclusion

A theoretical model describing the influence of damper addition on an initially unstable thermoacoustic system is presented. The parameters required to use the model for practical configurations like gas turbine combustors can be obtained by means of modal identification techniques. The eigenfrequencies and growth rates of the unstable system are extracted in this way, and the damper design and implementation can be optimized by estimating the growth rate reduction which would be obtained with these dampers. This model is first validated experimentally by means of an newly developped testing method. A thermoacoustic instability is mimicked by using an unstable electro-acoustic system in order to investigate the influence of dampers addition on its stability.

---

one can write

$$\omega_1 = -\alpha \left(\frac{\partial G/\partial \alpha}{\partial G/\partial \omega} \right)_{\omega_0,0} \text{ which yields } \omega = \omega_0 + i\frac{\alpha}{\tau_L} e^{i\omega_0\tau_F} e^{-i\omega_0\tau_L}$$

[5] This expression is a simplified form obtained by considering $\tau_F \ll \tau_L$ which valid for high order modes.

This is a pre-print version. Published in *Journal of Sound and Vibration* (2012) Vol. 331 (12), p. 2753-2763, DOI: 10.1016/j.jsv.2012.02.005

It consists in supplying a loudspeaker with a filtered-amplified-delayed microphone signal in a resonant cavity to reproduce the acoustic characteristics of a given thermoacoustic instability. It appears from the experiments that when the growth rates with and without damper are plotted against each other, they form an elongated ellipse. It is shown that the theory predicts a straight line which coincide with the major axis of this latter ellipse. This result indicates that the model successfully provides the mean growth rate reduction induced by the damper addition. Experimental results are supported by acoustic network simulations which are used to explain the differences between theoretical and measured growth rates. It is shown that the lower the amplification, the more narrow is the ellipse, and the better is the theoretical straight line approximation. One can incidentally note that one of the underlying assumptions of the theory is that the amplification is sufficiently weak, and hence does not influence the resonance frequency.
Beyond this model validation, the present experimental technique constitutes a new way to assess acoustic dampers prior to engine application. The work presented here focus on linear regimes, nevertheless, the damping performances in case of nonlinear regimes (strong acoustic levels which alter the flame response and modify the acoustic energy absorption characteristics of the dampers) can also be analysed with this new method. Also, despite the experimental validation is here performed with a simple non-reactive electro-acoustic system, the theoretical model can be used to estimate growth rate reductions in the case of complex geometries and reactive flows.

References

[1] Bellucci V., B. Schuermans, D. Nowak, P. Flohr and C. O. Paschereit, Thermoacoustic modeling of a gas turbine combustor equipped with acoustic dampers, Journal of Turbomachinery, 2005, **127**, 372–379.

[2] Dupère I. D. J. and A. P. Dowling, The use of Helmholtz resonators in a practical combustor, Journal of Engineering for Gas Turbines and Power, ASME Trans., 2005, **127**, 268–275.

[3] Tran N., S. Ducruix and T. Schuller, Analysis and control of combustion Instabilities by adaptative reflection coefficients, AIAA paper, 13^{th} AIAA/CEAS Aeroacoustics Conference, 28^{th} AIAA Aeroacoustics Conference, 2007, 1–12.

[4] Richards, G. A., Straub, D. L. and Robey, E. H., Passive Control of Combustion Dynamics in Stationary Gas Turbines, J. Prop. Power, 2003, **19** (5), 795–810.

[5] Huang, Y. and Yang, V., Dynamics and stability of lean-premixed swirl-stabilized combustion, Progress in Energy and Combustion Science, 2009, **35** (5), 293–364.

[6] Cummings, A., The effects of a resonator array on the sound field in a cavity, Journal of Sound and Vibration, 1992, **154**, 25–44.

[7] Park, J. H. and Sohn, C. H., On optimal design of half-wave resonators for acoustic damping in an enclosure, Journal of Sound and Vibration, 2009, **319**, 807–821.

[8] Li, D. and Cheng, L., Acoustically coupled model of an enclosure and a Helmholtz resonator array, Journal of Sound and Vibration, 2007, **305**, 272–288.

[9] Kim, H.J., Cha, J.-P., Song, J.-K. and Ko, Y.S., Geometric and number effect on damping capacity of Helmholtz resonators in a model chamber,J. Sound & Vib., 2010, doi: 10.1016/j.jsv.2010.02.018

[10] Morse P. M. and K. U. Ingard, Theoretical Acoustics, McGraw-Hill, New York, 1968.

This is a pre-print version. Published in *Journal of Sound and Vibration* (2012) Vol. 331 (12), p. 2753-2763, DOI: 10.1016/j.jsv.2012.02.005

[11] Nagaraja, S., Kedia, K. and Sujith, R.I., Characterizing energy growth during combustion instabilities: Singularvalues or eigenvalues, Proc. Comb. Inst., 2009, **32**, 2933–2940.

[12] Nicoud, F., Benoit, L., Sensiau, C. and Poinsot, T., Acoustic Modes in Combustors with Complex Impedances and Multidimensional Active Flames,AIAA J., 2007, **45**(2), 426–441.

[13] Culick F. E. C., Unsteady motions in combustion chambers for propulsion systems, AGARDograph, NATO/RTO-AG-AVT-039, 2006.

[14] Noiray N., D. Durox, T. Schuller and S. Candel, A unified framework for nonlinear combustion instability analysis based on the flame describing function, Journal of Fluid Mechanics, 2008, **615**, 139–167.

[15] Rienstra, S.W. and A. Hirschberg, An Introduction to Acoustics, Report IWDE 92-06, Eindhoven University of Technology, 2005.

[16] Schuermans, B., Guethe, F., Pennel, D., Guyot, D. and Paschereit, C. O., Thermoacoustic modeling of a gas turbine using transfer functions measured at full engine pressure,Proceedings of the ASME Turbo Expo 2009, Orlando, USA.

This is a pre-print version. Published in *Journal of Sound and Vibration* (2012) Vol. 331 (12), p. 2753-2763, DOI: 10.1016/j.jsv.2012.02.005